Doo-Sabin Surface Models with Biomechanical Constraints for Kalman Filter Based Endocardial Wall Tracking in 3D+T Echocardiography

Engin Dikici[1]
engin.dikici@ntnu.no
Fredrik Orderud[2]
fredrik.orderud@ge.com
Gabriel Kiss[1]
gabriel.kiss@ntnu.no
Anders Thorstensen[1]
anders.thorstensen@ntnu.no
Hans Torp[1]
hans.torp@ntnu.no

[1] Norwegian University of Science and Technology
Trondheim, Norway

[2] GE Vingmed Ultrasound
Oslo, Norway

Abstract

In this paper, a 3D left ventricle (LV) tracking framework utilizing Doo-Sabin subdivision surface models is extended with biomechanically constrained state transitions. First, an isoparametric finite element analysis (FEA) method for Doo-Sabin surface models is provided. The isoparametric FEA produces a stiffness matrix for a given endocardial model directly, eliminating inconvenient remodeling/meshing procedures commonly conducted prior to FEA. The computed model might lead to inaccurate deformation modes during the tracking due to hypothesized model shape and FEA parameters. Accordingly, we introduce a statistical model improvement approach for modifying the model shape and its stiffness matrix using experimentally observed endocardial surface variations. Finally, the state prediction stage of the Kalman tracking framework is formulated to perform constrained tracking. Comparative analyses show that the biomechanical constraints can significantly improve the endocardium tracking accuracy of the models with high control node resolutions.

1 Introduction

This paper considers the problem of endocardial border tracking in 3D+T echocardiography recordings. This is a challenging task due to reasons including speckle noise, shadowing, and the existence of intra-cavity structures (e.g. chordae tendineae, papillary muscles and valves) []. Furthermore, real-time detection of endocardial borders might be desirable during invasive procedures and intensive care applications.

http://dx.doi.org/10.5244/C.26.33

State-space analysis using Kalman filtering can be employed for the detection of left ventricle (LV) structures in time-dependent recordings. A Kalman filtering framework for tracking B-spline models was first introduced by Blake et al. [4]. This framework was later utilized for rapid tracking of LV in long-axis 2D echocardiography in [10, 11]. Orderud et al. extended the approach with the use of Doo-Sabin subdivision models for real-time tracking of 3D echocardiography recordings [12]. These studies took advantage of compact model representations for rapid tracking, but did not utilize physical properties to constrain model deformations. Liu et al. introduced a biomechanical-model constrained state-space analysis framework for the tracking of short-axis 2D echocardiography recordings [13]. Their study used *dense* Delaunay triangulated models and employed basic tri-nodal linear elements during the finite element analysis (FEA). Due to the triangulated high resolution model representations, it offered a computationally expensive solution.

The motivation for our study is to combine the compact model representations with biomechanical constraints for rapid and accurate tracking. To our knowledge, no work has been published on the biomechanically constrained tracking of subdivision surfaces using a Kalman filter. Accordingly, we extend the real-time Kalman tracking framework defined in [14] by employing biomechanically constrained state transitions. First, the isoparametric FEA method for Doo-Sabin surface models [7] is briefly described. This step enables the computation of a stiffness matrix for a given Doo-Sabin endocardial model using shell elements without changing the model geometry. It also eliminates the inconvenient remodeling/meshing procedures commonly conducted prior to FEA. However, the computed model might lead to inaccurate deformation modes due to hypothesized model shape and FEA parameters (e.g. Young's modulus, Poisson's ratio). The statistical model improvement stage addresses this problem by employing Control Point Distribution Models (CPDM) [6] and Baruch and Bar-Itzhack direct matrix modifications (BBDMM) [2]. It generates a more accurate model shape, and restricts model's deformation modes using experimentally observed endocardial surface variations. To compute CPDM, we introduce a regressive conversion method from ground-truth endocardial surface meshes to Doo-Sabin surface representations. The mean endocardial surface model and its modes of deformation are found using Doo-Sabin surface representations that are converted from a training dataset. The mean shape is utilized as the new model shape, and the modes of deformation are used for modifying the model stiffness matrix in BBDMM method. Finally, the state prediction stage of the Kalman tracking framework is formulated to perform biomechanically constrained tracking. In the results section, endocardial surface tracking quality is compared among (1) Doo-Sabin surface models with different control node resolutions, (2) biomechanically constrained and non-constrained state transitions, and (3) the systems employing statistically improved and not improved Doo-Sabin models.

2 Isoparametric Formulation of Doo-Sabin Surface Models

The tracking framework introduced in [14] is built around a deformable Doo-Sabin subdivision model parametrized by a set of control nodes with associated displacement direction vectors. For the FEA of Doo-Sabin endocardial models, we propose to use an isoparametric method from [7] as it (1) eliminates the need for meshing tools by employing a unified geometric representation for the design and analysis, and (2) generates a stiffness matrix that is

directly defined for the control node displacements of the model.

A Doo-Sabin surface is a type of a subdivision surface that generalizes bi-quadric B-spline patches to an arbitrary topology [8]. It is defined as the limit surface of a recursive subdivision process. Each limit surface position of a patch is uniquely described using *parametric* patch coordinates (ξ, η) that vary between 0 and 1. The basis functions map patch coordinates to *physical* coordinates by,

$$\mathbf{y} = \sum_{i=1}^{n} b_i(\xi, \eta)\, \mathbf{q_i}, \tag{1}$$

where (1) n gives the total number of control nodes for a given patch, (2) b_i is the basis function for the i^{th} control node of the patch, (3) $\mathbf{q}_i$ gives the physical coordinates of the i^{th} control node, and (4) $\mathbf{y}$ holds the mapped physical coordinates. Please refer to [14] for the derivation of the basis functions.

The basis functions can also be utilized for defining isoparametric solid shell elements during the FEA [7]. The degenerated solids based approach, proposed in [1], can be employed for the shell elements with shape functions:

$$\mathbf{y} = \sum_{i=1}^{n} b_i(\xi, \eta) \left\{ \mathbf{q}_i + t\frac{\zeta}{2}\mathbf{v}_{3i} \right\}, \tag{2}$$

where (1) $[\mathbf{v}_{1i}, \mathbf{v}_{2i}, \mathbf{v}_{3i}]$ defines orthogonal axes at the i^{th} control node of the patch, in which $\mathbf{v}_{3i}$ gives the surface normal direction, (2) t gives the shell thickness, and (3) a parametric patch coordinate ζ traverses on the surface normal direction. Hence, each surface patch is represented by a shell element with a thickness. The displacement vector $\mathbf{u}$ of any point in the element is given by,

$$\mathbf{u} = \sum_{i=1}^{n} b_i(\xi, \eta) \left\{ \mathbf{u_i} + t\frac{\zeta}{2} [\mathbf{v}_{1i}, -\mathbf{v}_{2i}] \begin{bmatrix} \alpha_i \\ \beta_i \end{bmatrix} \right\}, \tag{3}$$

where (1) $\mathbf{u_i} = [u_i, v_i, w_i]^T$ is the displacement vector for the i^{th} control node, and (2) α_i and β_i are the scalar rotations in radians around $\mathbf{v}_{1i}$ and $\mathbf{v}_{2i}$ axes respectively. During the FEA of the shell structures, a *local* coordinate system (x', y', z') of the element needs to be determined. By applying a linear interpolation, an orthogonal set of local coordinate axes for any point in the element are given by,

$$\mathbf{v}_3(\xi, \eta) = \frac{\sum_{i=1}^{n} b_i(\xi, \eta)\, \mathbf{v}_{3i}}{|\sum_{i=1}^{n} b_i(\xi, \eta)\, \mathbf{v}_{3i}|}, \quad \mathbf{v}_1(\xi, \eta) = \frac{\mathbf{h} \times \mathbf{v}_3}{|\mathbf{h} \times \mathbf{v}_3|}, \quad \mathbf{v}_2(\xi, \eta) = \mathbf{v}_3 \times \mathbf{v}_1, \tag{4}$$

with $\mathbf{h}$ giving an arbitrary vector that satisfies $\mathbf{h} \neq \mathbf{v}_3(\xi, \eta)$.

The strain vector $\boldsymbol{\varepsilon} = \left[\varepsilon_{x'}, \varepsilon_{y'}, \gamma_{x'y'}, \gamma_{x'z'}, \gamma_{y'z'}\right]^T$ is described by the first partial derivatives of the local displacement vector $\mathbf{u}' = [u', v', w']^T$ as

$$\boldsymbol{\varepsilon} = \begin{bmatrix} \frac{\partial u'}{\partial x'}, & \frac{\partial v'}{\partial y'}, & \frac{\partial u'}{\partial y'} + \frac{\partial v'}{\partial x'}, & \frac{\partial u'}{\partial z'} + \frac{\partial w'}{\partial x'}, & \frac{\partial v'}{\partial z'} + \frac{\partial w'}{\partial y'} \end{bmatrix}^T, \tag{5}$$

where (1) $\varepsilon_{x'}$ and $\varepsilon_{y'}$ are the normal strains in x' and y' directions, and (2) $\gamma_{x'y'}$, $\gamma_{x'z'}$ and $\gamma_{y'z'}$ are the shear strains in the $x'y'$, $x'z'$ and $y'z'$ planes respectively. The relation between the strain and stress (σ) vectors can be formed using *Generalized Hooke's Law* as $\sigma = \mathbf{D}\varepsilon$, in which the material matrix $\mathbf{D}$ is defined using Young's modulus and Poisson's ratio [1].

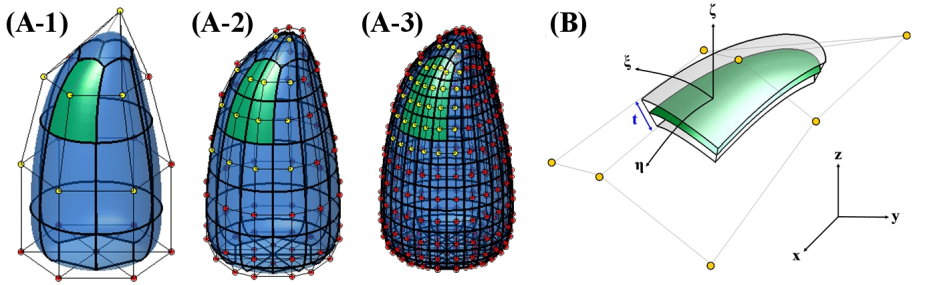

Figure 1: (A) The limit surface of an arbitrary patch and its subdivisions are shown in green, the control nodes for the green patches are shown in yellow. Subdivided patches define the exact same limit surface as the original patch. (B) The geometry of a shell element for the green patch from (A-1) is shown; each patch is modeled by a shell element.

Using a variational formulation, the stiffness matrix of an element is given by:

$$\mathbf{K}_e = \iiint \mathbf{B}^T \mathbf{D} \mathbf{B} dx dy dz, \tag{6}$$

where $\mathbf{B}$ *(strain-displacement matrix)* relates the strains to the control node displacements *(δ)* using $\varepsilon = \mathbf{B}\delta$. To compute $\mathbf{B}$, firstly the components of ε are found as described in [7]. Next, $\mathbf{B}$ can be found solving $\varepsilon = \mathbf{B}[\delta_1, \delta_2, \ldots \delta_n]^T$ where $\delta_i = [u_i, v_i, w_i, \alpha_i, \beta_i]^T$. The infinitesimal volume computed in physical coordinates can be expressed in terms of parametric coordinates as $dxdydz = |\mathbf{J}| d\xi d\eta d\zeta$, in which 3×3 Jacobian matrix $\mathbf{J}$ gives the first-order partial derivatives of physical coordinates with respect to parametric coordinates. Finally, $\iiint \mathbf{B}^T \mathbf{D} \mathbf{B} |\mathbf{J}| d\xi d\eta d\zeta$ can be numerically estimated using Gauss Legendre quadrature rules. Using two samples in ζ direction and minimum four samples in both ξ and η directions is sufficient for thin shell element stiffness matrix calculations [1]. Computed element stiffness matrices can be assembled into a model stiffness matrix $\mathbf{K}$ following a standard procedure.

The resolution of a given Doo-Sabin surface model can be adjusted by basis refinements, without changing the model geometry or its parametrization (See Figure 1). A Doo-Sabin surface refinement produces a model with a higher number of elements, which provides an increased physical simulation accuracy during FEA. The convergence properties of Doo-Sabin shell elements are reported in [7].

3 Statistical Model Improvements

An endocardial model designed using hypothetical shape and material properties (e.g. Young's modulus and Poisson's ratio) might lead to poor tracking accuracy. Yet, the identification of the optimal properties requires a considerable amount of user input and time, which might not be manageable for a complex structure such as the LV [3]. We propose to use a statistical model improvement method that (1) learns the mean model shape and its deformations using a training dataset, and (2) updates the model shape and the stiffness matrix directly using the learned information.

For producing a statistical endocardial Doo-Sabin surface model, firstly a conversion procedure between 3D ground-truth endocardial surface segmentations and Doo-Sabin surface representations needs to be described. We propose a regressive approach for this task.

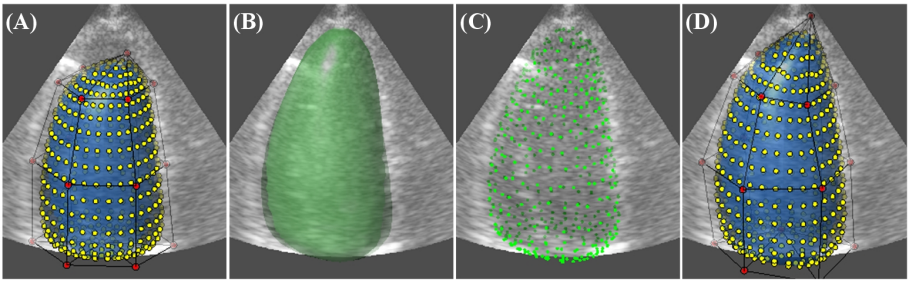

Figure 2: (A) Doo-Sabin surface representation produced by the classical tracker with landmark (yellow) and control (red) points, which does not fit at apical region, (B) ground-truth surface segmentation, (C) ground-truth landmark points, and (D) updated Doo-Sabin surface representation using MLE based conversion are represented.

A dense set of landmark points ($m \gg n$), which are evenly spread around a patch, is given by $L = \{(\xi_1, \eta_1), (\xi_2, \eta_2), \ldots, (\xi_m, \eta_m)\}$. The tracker defined in [14], referred as the *classical tracker*, maps L on to a set of Cartesian coordinates as $(\xi_i, \eta_i) \rightarrow \mathbf{y_i}^{(\rho,\tau)}$, where (1) $\rho \in \{1, 2, \ldots r\}$ identifies a recording, and (2) $\tau \in [0 : \text{end-systole}, 1 : \text{end-diastole}]$ gives the temporal cardiac cycle position. Each $\mathbf{y_i}^{(\rho,\tau)}$ can be updated using a normal displacement *(in* $\mathbf{v}_3$ *direction from Equations 4)* to a ground-truth surface point $\tilde{\mathbf{y}}_i^{(b,\tau)}$. Next, m equations that relate unknown patch control node positions, $\mathbf{q}^{(\rho,\tau)}$, and the ground-truth surface points can be defined as,

$$\tilde{\mathbf{y}}_i^{(\rho,\tau)} = \sum_{j=1}^{n} b_j(\xi_i, \eta_i)\, \mathbf{q}_j^{(\rho,\tau)}, \quad 1 \leq i \leq m. \tag{7}$$

The equations collected from all surface patches can be put into a matrix form:

$$\tilde{\mathbf{Y}}^{(\rho,\tau)} = \mathbf{F}\mathbf{Q}^{(\rho,\tau)} + \mathbf{W}, \tag{8}$$

where (1) $\mathbf{F}$ is a design matrix holding the basis function values, (2) $\mathbf{Q}^{(\rho,\tau)}$ is a model control node matrix, and (3) $\mathbf{W}$ is a mapping error matrix. Assuming white mapping errors, the maximum likelihood estimator (MLE) for $\mathbf{Q}^{(\rho,\tau)}$ is found by $\hat{\mathbf{Q}}^{(\rho,\tau)} = \left(\mathbf{F}^T\mathbf{F}\right)^{-1}\mathbf{F}^T\tilde{\mathbf{Y}}^{(\rho,\tau)}$ [12]. A Doo-Sabin surface representation with the control nodes given by $\hat{\mathbf{Q}}^{(\rho,\tau)}$ fits onto the ground-truth endocardial surface segmentation for the recording ρ at τ (see Figure 2).

After estimating Doo-Sabin surface representations for all training recordings at each cardiac cycle position, CPDM can be computed. First, the surface representations are aligned utilizing the global state information of the classical tracker, which keeps the model translation and rotation with respect to an initial model state [14]. Next, the mean model representation is computed using the aligned models; $\bar{\mathbf{Q}}$ gives the mean model's control nodes. Finally, the control node covariance matrix $\mathbf{V}$ about $\bar{\mathbf{Q}}$ is found. The t eigenvectors of $\mathbf{V}$, $\mathbf{S} = [\mathbf{s}_1, \mathbf{s}_2, \ldots, \mathbf{s}_t]$, corresponding to the largest t eigenvalues $\Omega_{pdm}^2 = diag\left(\omega_1^2, \omega_2^2, \ldots, \omega_t^2\right)$, give the observed modes of variation (or deformation) for the model [8].

The Doo-Sabin model employed in the classical tracker can be improved using (1) the mean model representation, and (2) the observed modes of deformation. First, the model control nodes are modified as the mean model control nodes $\bar{\mathbf{Q}}$, hence the modes of deformation of the observed and computed models are comparable. Then, the model stiffness

matrix for the modified model is found using the isoparametric formulation introduced in the previous section as $\mathbf{K}^{'}$. *Modal Analysis* can be performed to find deformation modes of the modified model by solving,

$$\mathbf{K}^{'}\Phi_{fem} = \mathbf{M}\Phi_{fem}\Omega^2_{fem}, \tag{9}$$

where (1) $\mathbf{M}$ is a mass matrix assumed as an identity matrix in our study, (2) Φ_{fem} is the eigenvector matrix of $\mathbf{M}^{-1}\mathbf{K}^{'}$ and represents the deformation modes, and (3) Ω^2_{fem} is a diagonal matrix of the associated eigenvalues. It is desirable to have similar deformation modes as the observed ones given by CPDM.

The BBDMM is a direct matrix modification method [2] that makes minimal amount of modifications on the original stiffness matrix to produce desired deformation modes. In this study, it is utilized to make minimal modifications to $\mathbf{K}'$ by solving,

$$\begin{aligned} min_{\mathbf{K}_{opt}} & \left\| \mathbf{M}^{-1/2}\left(\mathbf{K}_{opt} - \mathbf{K}^{'}\right)\mathbf{M}^{-1/2} \right\|_F, \\ s.t. \quad & \mathbf{K}_{opt}\mathbf{S} = \mathbf{M}\mathbf{S}\Omega^2_{pdm}, \qquad \mathbf{K}_{opt} = \mathbf{K}^T_{opt}, \end{aligned} \tag{10}$$

where $\|\cdot\|_F$ is the Frobenius norm. With the assumptions of (1) $\mathbf{K}^{'}$ is symmetric, (2) $\mathbf{S}$ and $\mathbf{M}\mathbf{S}\Omega^2_{pdm}$ are both full rank, (3) $\mathbf{S}^T\mathbf{M}\mathbf{S}\Omega^2_{pdm}$ is symmetric and non-singular, and (4) $\mathbf{M}$ is non singular such that $Rank\left(\mathbf{M}^T\mathbf{M}\mathbf{S}\right) = Rank\left(\mathbf{M}\mathbf{S}\Omega^2_{pdm}\right)$, the unique solution to $\mathbf{K}_{opt}$ can be found as,

$$\begin{aligned} \mathbf{K}_{opt} = \mathbf{K}^{'} &+ \left(\mathbf{Y} - \mathbf{K}^{'}\mathbf{S}\right)\left(\mathbf{Y}^T\mathbf{S}\right)^{-1}\mathbf{Y}^T + \mathbf{Y}\left(\mathbf{S}^T\mathbf{Y}\right)^{-1}\left(\mathbf{Y} - \mathbf{K}^{'}\mathbf{S}\right)^T \\ &- \mathbf{Y}\left(\mathbf{Y}^T\mathbf{S}\right)^{-1}\left(\mathbf{Y} - \mathbf{K}^{'}\mathbf{S}\right)^T\mathbf{S}\left(\mathbf{Y}^T\mathbf{S}\right)^{-1}\mathbf{Y}^T, \end{aligned} \tag{11}$$

where $\mathbf{Y} = \mathbf{M}\mathbf{S}\Omega^2_{pdm}$ [3], and $\mathbf{K}_{opt}$ is the optimally modified stiffness matrix for the endocardial model. Please note that $\mathbf{S}$ gives the t most prominent deformation modes for $\mathbf{K}_{opt}$: the major deformation modes produced by $\mathbf{K}_{opt}$ are similar with the observed modes learned from a training dataset.

4 Tracking Framework

The tracking framework represents the shape and pose deformations by a composite transform, where local shape deformations are obtained by moving control nodes in the subdivision model together with a global transformation that translates, rotates and scales the whole model. This leads to a composite state vector $\mathbf{x} = \left[\mathbf{x}_g^T, \mathbf{x}_l^T\right]^T$, consisting of n_g global and n_l local parameters.

The tracking framework consists of five separate stages, namely the (1) state prediction, (2) evaluation of tracking model, (3) edge measurements, (4) measurement assimilation, and (5) measurement update. The biomechanical constraints can be enforced in the state prediction stage [13], which is further elaborated in this section. A more detailed discussion on the other stages of the framework can be found in [14].

The control node displacements of a Doo-Sabin surface model can be formulated under the principle of minimal energy using ordinary differential equation as,

$$\mathbf{M}\ddot{\mathbf{u}} + \mathbf{C}\dot{\mathbf{u}} + \mathbf{K}\mathbf{u} = \mathbf{0}, \tag{12}$$

where (1) $\mathbf{u} = [u_1, u_2, \ldots, u_p]^T$ gives the normal displacements for a model with p control nodes, and (2) $\mathbf{C}$ is a *Rayleigh* damping matrix, which can be found by $\mathbf{C} = \alpha\mathbf{M} + \beta\mathbf{K}$ with small weighting constants α and β. Accordingly, a continuous-time linear time-invariant stochastic system can be derived as $\dot{\mathbf{x}}(t) = \mathbf{A}_c\mathbf{x}(t)$, where

$$\mathbf{x}[t] = \begin{bmatrix} \mathbf{u}(t) \\ \dot{\mathbf{u}}(t) \end{bmatrix}, \quad \mathbf{A}_c = \begin{bmatrix} \mathbf{0} & \mathbf{I} \\ -\mathbf{M}^{-1}\mathbf{K} & -\mathbf{M}^{-1}\mathbf{C} \end{bmatrix}. \tag{13}$$

This system can be discretized as $\mathbf{x}[k+1] = \mathbf{A}_d\mathbf{x}[k]$, where (1) $\mathbf{x}[k] = \left[\mathbf{u}[k]^T \ \mathbf{v}[k]^T\right]^T$ with $\mathbf{v}[k]$ denoting the velocities of the control nodes at time step k, and (2) $\mathbf{A}_d = e^{\mathbf{A}_c\Gamma}$ where $\Gamma = 1$ gives the unit sampling interval used in our study. $\mathbf{A}_d$ can be decomposed as,

$$\mathbf{A}_d = \begin{bmatrix} \mathbf{A}_{00} & \mathbf{A}_{01} \\ \mathbf{A}_{10} & \mathbf{A}_{11} \end{bmatrix}, \tag{14}$$

where $\mathbf{A}_{00}$, $\mathbf{A}_{01}$, $\mathbf{A}_{10}$ and $\mathbf{A}_{11}$ are $p \times p$ sub-matrices. Assuming $\mathbf{v}[k] \approx \frac{\mathbf{u}[k]-\mathbf{u}[k-1]}{\Gamma}$, the motion model can be written in terms of the last two successive states as,

$$\mathbf{u}[k+1] = \left[\mathbf{A}_{00} + \Gamma^{-1}\mathbf{A}_{01}\right]\mathbf{u}[k] + \left[-\Gamma^{-1}\mathbf{A}_{01}\right]\mathbf{u}[k-1]. \tag{15}$$

In [14], control nodes' normal displacements give the system local states; $\mathbf{x}_l = \mathbf{u}$. Hence, Equation 15 can be directly plugged into the joint motion model proposed in [14] by,

$$\bar{\mathbf{x}}[k+1] = \begin{bmatrix} \mathbf{R}_g & \mathbf{0} \\ \mathbf{0} & \mathbf{R}_l\left(\mathbf{A}_{00} + \Gamma^{-1}\mathbf{A}_{01}\right) \end{bmatrix}\hat{\mathbf{x}}[k] + \begin{bmatrix} \mathbf{0} & \mathbf{0} \\ \mathbf{0} & \mathbf{R}_l\left(-\Gamma^{-1}\mathbf{A}_{01}\right) \end{bmatrix}\hat{\mathbf{x}}[k-1], \tag{16}$$

where (1) $\bar{\mathbf{x}}[k+1]$ is the predicted state for the time step $k+1$, (2) $\hat{\mathbf{x}}[k]$ is the estimated state from the time step k, and (3) $\mathbf{R}_g$ and $\mathbf{R}_l$ are the regularization matrices for the global and local state parameters respectively.

5 Results

3D echocardiography was performed on 10 healthy subjects and 19 subjects with recent first time myocardial infarction, using a Vivid 7 (26 recordings) or a Vivid E9 (3 recordings) ultrasound scanner (GE Vingmed Ultrasound, Norway) with a matrix array (3V) transducer. The endocardial border segmentation of the recordings was performed by a trained medical doctor using a semi-automatic segmentation tool (4D AutoLVQ, GE Vingmed Ultrasound, Norway).

For the initial FEA, the shell thickness, Young's modulus and Poisson's ratio were set as $8mm$, $75000Pa$ and 0.47 as proposed in [13]. For the CPDM based model updates, a set of 441 landmark points evenly spread around the model was used. The observed modes of deformation were represented using five eigenvectors $(t = 5)$ corresponding to the five largest

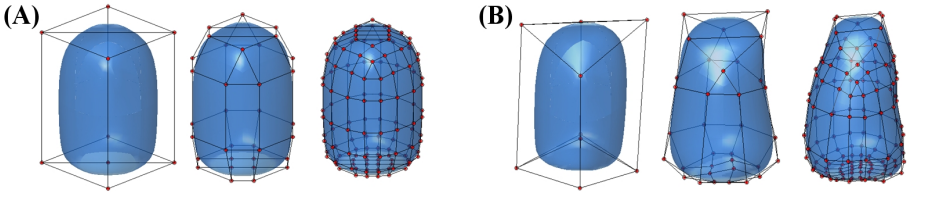

Figure 3: Not-refined, refined and double-refined Doo-Sabin surface models (A) for the *noBC* and *BCnoI* , and (B) *BCwithI* setups are represented. For the *BCwithI*, control node positions are updated using the mean model computed by CPDM.

eigenvalues, which described $\geq 90\%$ of the experimentally observed endocardial shape variations. The Rayleigh damping constants of the tracker were set as $\alpha = \beta = 0.1$.

The Kalman tracking framework was evaluated for three different configurations:

1. The system with no biomechanical constraints *(noBC)*: it tracks a Doo-Sabin surface model using a tracker with no biomechanical constraints. This setup is identical with the classical tracker [14].

2. The system with biomechanical constraints and no statistical model improvements *(BCnoI)*: it tracks a Doo-Sabin surface model using a tracker with biomechanically constrained state transitions, as described in Section 4. The model's stiffness matrix was computed using the isoparametric FEA method from Section 2.

3. The system with biomechanical constraints and statistical model improvements *(BCwithI)*: it tracks an improved Doo-Sabin surface model using a tracker with biomechanically constrained state transitions. The improved model has a modified shape and a stiffness matrix as described in Section 3.

Each configuration was executed with not-refined (9 nodes), refined (34 nodes) and double-refined (136 nodes) Doo-Sabin surface models represented in Figure 3. *noBC* and *BCnoI* setups were tested using all 29 recordings directly. As *BCwithI* requires a training with a pre-segmented dataset, it was tested via leave-one-out cross-validation [9]. The error measurements including the (a) *absolute surface point error* giving the average absolute distance of each predicted surface point to ground-truth surface, (b) *squared surface point error* giving the average squared distance of each predicted surface point to ground-truth surface, and (c) *absolute volume error* giving the average of predicted surface's absolute volume errors are given in Figure 4. *Signed surface error polar plots*, showing the average signed distances between the predicted and ground-truth surfaces using 17-segment model of the American Heart Association [5], are represented in Figure 5. There were no significant differences between the segmentation performances for the subjects with and without infarction; therefore, the evaluation results are reported for all recordings without any further classification.

The tracking framework is implemented in C++, and processes each frame in 2*ms* with not-refined, 3.4*ms* with refined and 30.6*ms* with double-refined models when executed on a 2.80 GHz Intel Core 2 Duo CPU. There are no execution time differences between the *noBC*, *BCnoI* and *BCwithI* setups as the stiffness and state transition matrices are computed only once for each model.

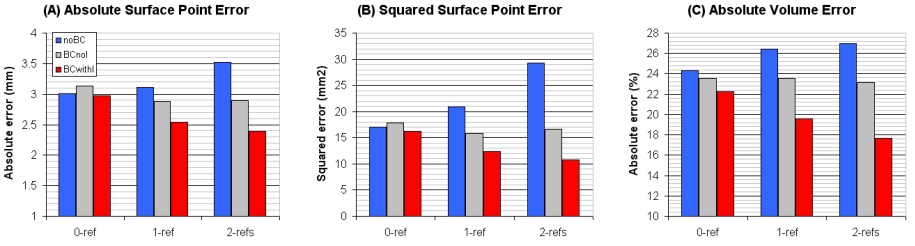

Figure 4: (A) Absolute surface point error (in *mm*) , (B) squared surface point error (in mm^2), and (C) absolute volume error (in percentages) for the Kalman tracking framework with *noBC*, *BCnoI*, and *BCwithI* setups for non-refined, refined and double-refined Doo-Sabin model tracking.

6 Discussion and Conclusion

In this study, we extended the real-time Doo-Sabin surface models based Kalman tracking framework with biomechanical constraints. The introduced method is (1) practical; the computed models can be directly used in a Kalman tracking framework by implementing a few modifications in the state prediction stage, (2) useful since it improves the tracking accuracy without introducing additional run-time complexity, (3) yet novel as the biomechanically constrained subdivision surfaces have not been employed in a Kalman tracker prior to our study.

Our analyses showed that the biomechanical constraints are necessary especially when the tracked model has a high control node resolution. This is due to the fact that as the model complexity increases the tracker can benefit more from a spatial regularization, which is provided by biomechanical constraints. Hence, we can observe that the *BCnoI* setup allows tracking quality to be stabilized over model resolution levels (see Figure 4 and Figure 5 row-2). The statistical model improvements take advantage of higher model resolution levels as (1) the model node updates provide a more realistic model shape to perform tracking, and (2) deformation modes learned from CPDM improve the stiffness matrix accuracy (see Figure 4 and Figure 5 row-3).

The 17-segment model representations show that the initial tracker produces significant under-estimation error (estimated borders are closer to the object center than the ground-truth borders) at the apex region, the center of the polar plot (see Figure 5 row-1). Introducing biomechanical constraints or increasing the model resolution without changing the model shape does not significantly improve the tracking accuracy for the apex region (see Figure 5 row-2). The model improvement stage alleviates the problem by modifying the model shape to have a curvier apical part, which is closer to the natural appearance of the LV (see Figure 3 (B) and Figure 5 row-3).

References

[1] S. Ahmad, B. M. Irons, and O. C. Zienkiewicz. Analysis of thick and thin shell structures by curved finite elements. *International Journal for Numerical Methods in Engineering*, 2(3):419–451, 1970. ISSN 1097-0207. doi: 10.1002/nme.1620020310.

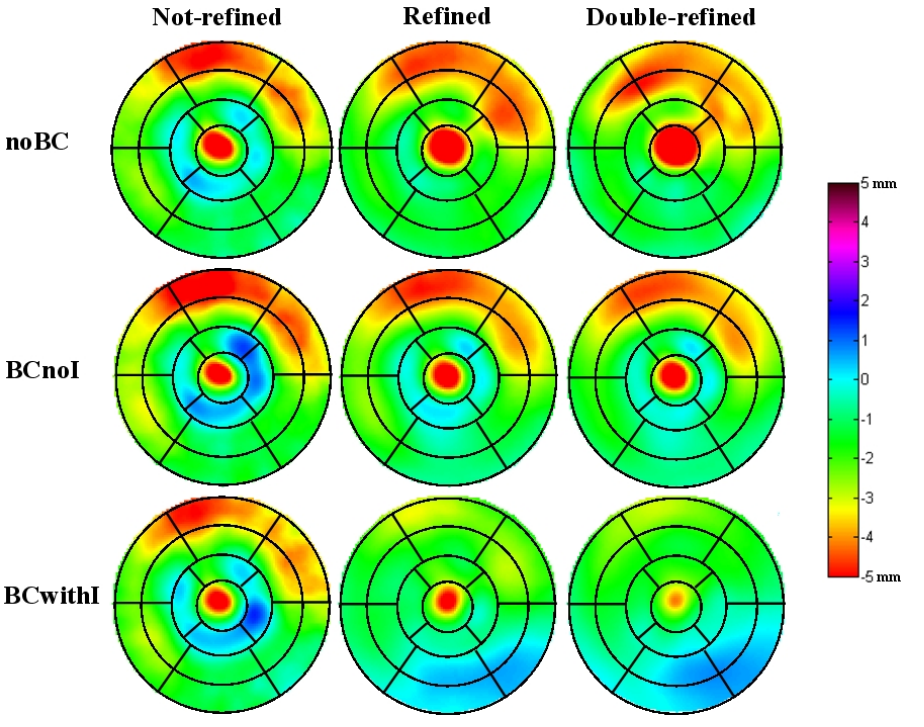

Figure 5: 17-segment model representations for the signed surface error: 5*mm* over-estimation is purple, 5*mm* under-estimation is red, 0*mm* no-error is light blue. Rows 1, 2 and 3 show the error plots for the *noBC*, *BCnoI*, and *BCwithI* setups respectively. Columns 1, 2 and 3 show the error plots for the non-refined, refined and double-refined Doo-Sabin model trackers respectively.

[2] M. Baruch and I. Y. Bar Itzhack. Optimal weighted orthogonalization of measured modes. *AIAA Journal*, 16(4):346–351, 1978.

[3] C. A. Beattie and S. W. Smith. Optimal matrix approximants in structural identification. *Journal of Optimization Theory and Applications*, 74:23–56, 1992. ISSN 0022-3239. URL http://dx.doi.org/10.1007/BF00939891. 10.1007/BF00939891.

[4] A. Blake and M. Isard. *Active contours: the application of techniques from graphics, vision, control theory and statistics to visual tracking of shapes in motion*. Springer-Verlag New York, Inc., Secaucus, NJ, USA, 1998. ISBN 3540762175.

[5] M. D. Cerqueira, N. J. Weissman, V. Dilsizian, et al. Standardized myocardial segmentation and nomenclature for tomographic imaging of the heart: a statement for healthcare professionals from the Cardiac Imaging Committee of the Council on Clinical Cardiology of the American Heart Association. . *Circulation*, 105(4): 539–542, January 2002. ISSN 1524-4539. doi: 10.1161/hc0402.102975. URL http://dx.doi.org/10.1161/hc0402.102975.

[6] T. F. Cootes, C. J. Taylor, D. H. Cooper, and J. Graham. Training models of shape from sets of examples. In *In Proc. British Machine Vision Conference*, pages 9–18, 1992.

[7] E. Dikici, S. R. Snare, and F. Orderud. Isoparametric finite element analysis for doo-sabin subdivision models. In *Proceedings of Graphics Interface 2012*, GI '12, Toronto, Ont., Canada, Canada, 2012. Canadian Information Processing Society.

[8] D. Doo and M. Sabin. Behaviour of recursive division surfaces near extraordinary points. *Computer-Aided Design*, 10(6):356 – 360, 1978. ISSN 0010-4485. doi: 10.1016/0010-4485(78)90111-2.

[9] T. Hastie, R. Tibshirani, and J.H. Friedman. *The elements of statistical learning: data mining, inference, and prediction*. Springer series in statistics. Springer, 2009. ISBN 9780387848570. URL http://books.google.com/books?id=tVIjmNS3Ob8C.

[10] G. Jacob, J. A. Noble, M. M. Parada, and A. Blake. Evaluating a robust contour tracker on echocardiographic sequences. *Medical Image Analysis*, 3(1):63 – 75, 1999. ISSN 1361-8415. doi: DOI:10.1016/S1361-8415(99)80017-6.

[11] G. Jacob, J.A. Noble, C. Behrenbruch, A.D. Kelion, and A.P. Banning. A shape-space-based approach to tracking myocardial borders and quantifying regional left-ventricular function applied in echocardiography. *Medical Imaging, IEEE Transactions on*, 21(3):226 –238, march 2002. ISSN 0278-0062. doi: 10.1109/42.996341.

[12] S. M. Kay. *Fundamentals of statistical signal processing: estimation theory*. Prentice-Hall, Inc., Upper Saddle River, NJ, USA, 1993. ISBN 0-13-345711-7.

[13] H. Liu and P. Shi. State-space analysis of cardiac motion with biomechanical constraints. *Image Processing, IEEE Transactions on*, 16(4):901–917, March 2007. doi: 10.1109/TIP.2007.891773. URL http://dx.doi.org/10.1109/TIP.2007.891773.

[14] F. Orderud and S. I. Rabben. Real-time 3d segmentation of the left ventricle using deformable subdivision surfaces. In *CVPR*, 2008.

[15] S. K. Setarehdan and John J. Soraghan. *Segmentation in echocardiographic images*, pages 64–130. Springer-Verlag New York, Inc., New York, NY, USA, 2002. ISBN 1-85233-389-8.